How octopus arm muscle contractile properties and anatomical organization contribute to the arm functional specialization

Letizia Zullo[1,2*], Alessio Di Clemente[1,3*], Federica Maiole[1,3]

[1]Center for Micro-BioRobotics & Center for Synaptic Neuroscience and Technology (NSYN), Istituto Italiano di Tecnologia, Largo Rosanna Benzi 10, 16132 Genova, Italy

[2] IRCSS, Ospedale Policlinico San Martino, Largo Rosanna Benzi 10, 16132 Genova, Italy

[3] Department of Experimental Medicine, University of Genova, Viale Benedetto XV, 3, 16132 Genova, Italy

[*]equal contribution

[‡]Author for correspondence: letizia.zullo@iit.it

Key words: muscle biomechanics, octopus, motor control, invertebrate muscles, muscular hydrostat, force-length relationship

Summary statement

Octopus arm functional properties emerge from muscle contractile properties and limb anatomical organization and underpin behavioral ‘specialization’ of arm portions.

Abstract

Octopus arms are highly flexible structures capable of complex motions and are used in a wide repertoire of behaviors. Movements are generated by the coordinated summation of innervation signals to packed arrays of muscles oriented in different directions and moving based on their anatomical relationships. In this study, we investigated the interplay between muscle biomechanics and anatomical organization in

the *Octopus vulgaris* arm to elucidate their role in different arm movements. We performed isometric and isotonic force measurements on isolated longitudinal (L) and transverse (T) arm muscles and showed that L has a higher rate of activation and relaxation, lower twitch-to-tetanus ratio, and lower passive tension than T muscles, thus prompting their use as faster and slower muscles, respectively. This points to the use of L in more graded responses, such as those involved in precise actions, and T in intense and sustained actions, such as motion stabilization and posture maintenance. Once activated, the arm muscles exert forces that cause deformations of the entire arm, which are determined by the amount, location, properties and orientation of their fibers. Here, we show that, although continuous, the arm manifests a certain degree of morphological specialization, where the arm muscles have a different aspect ratio along the arm. This possibly supports the functional specialization of arm portion observed in various motions, such as fetching and crawling.

Hence, the octopus arm as a whole can be seen as a 'reservoir' of possibilities where different types of motion may emerge at the limb level through the co-option of the muscle contractile properties and structural arrangement.

Introduction

In animals, motion is achieved through the coordinated recruitment of specific muscles with an appropriate activation input. In addition, muscle anatomical positioning and the summation of innervation signals allow muscles to move relative to one another and produce limb motion. Hence, movement is determined by a fine interplay between motoneuronal inputs and the organization and type of innervated muscles. In vertebrate animals, the central nervous system activates, based on rigid body coordinates, selected motor brain areas to produce muscle synergies and efficiently accomplish a motor task. Soft-bodied animals have a body unconstrained by rigid skeletal elements, in which motion is obtained through the contraction of muscles against incompressible fluid or tissue, allowing structural deformation or stiffening (Taylor and Kier, 2003). It has been widely demonstrated that the morphological arrangement of muscles may significantly contribute to overall muscle function in a variety of hydrostatic organs (Kier,

2012; Kier, 2016; Uyeno and Kier, 2005). *Octopus vulgaris* arms are muscular hydrostats, where flexibility is coupled with a high precision of movement. They can actively elongate, bend, and twist through alternate or simultaneous activation of groups of obliquely striated muscles (Kier and Stella, 2007; Zullo et al., 2017). However, the extent to which arm dynamic deformation is dependent on limb-embedded muscular properties and centrally coordinated muscle activation is not yet understood. Central motor control in cephalopods has been functionally investigated in only a limited number of studies. In the octopus, it has been shown that, in the brain's higher motor centers, the absence of motor topographic maps is accompanied by a spatially distributed organization of motor components, allowing for the construction of a large variety of motions (Zullo and Hochner, 2011; Zullo et al., 2009).

In this study, we investigated the extent to which arm motion can emerge at the limb level through the functional and structural characteristics of the muscles comprising the arm.

To do so, we studied the interplay between arm muscle physiology and anatomical positioning, and elucidated how these factors may contribute to mechanically diverse arm functions.

We first performed an *in vitro* characterization of the active biomechanical properties of the two main muscle layers of the *Octopus vulgaris* arm bulk, namely the longitudinal (L) and transverse (T) muscles. We investigated their activation properties and force-length relationship to disclose the mechanical principles underlying force and movement production, and to elucidate possible differences in the physiology of muscles occupying the inner to outer arm regions. The octopus arm muscles are functionally similar to vertebrate skeletal muscles. According to the sliding filament hypothesis, the force muscles generated upon activation is primarily related to their length and are described by the well-known force-length (F/L) curve. This relationship indicates that muscles generate the greatest force at values around their optimal length, often corresponding to the resting length in skeletal muscles, and decreasing forces at both longer and shorter lengths. While skeletal muscles manifest a small range of length variation due to their attachment to rigid structures (the bones) through tendons (for a review see (Burkholder

and Lieber, 2001)), the octopus arm poses a question in this regard as it is not constrained to a fixed length and undergoes large-scale deformations during motion. This allows arm muscles to theoretically work over different regions of their force-length curve depending on their strain level. This feature is particularly relevant in light of the findings of Di Clemente et al., who showed that hydrostatic pressure is inherently present in the octopus arm and affects both muscle strain and passive biomechanical response (Di Clemente et al., 2021). Moreover, strain variations can also influence the ability of the muscle to produce force, and therefore, its function during motion. Hence, muscle fiber contractile properties must be interpreted in light of the muscle architecture and anatomical arrangement.

According to the current literature, the octopus arm has a proximal-distal continuity of muscles, thus seemingly lacking regional diversification. However, evidence of a behavioral 'specialization' of arm portions has been found in various motions such as fetching, crawling, searching, and even constrained pulling. In these behaviors, the proximal, medial, and distal segments of the arm can be used preferentially or alternatively (Gutnick et al., 2011; Gutnick et al., 2020; Kennedy et al., 2020; Levy et al., 2015; Richter et al., 2015; Sumbre et al., 2005). However, the principles underlying this functional diversification remain unclear. To elucidate this point, we next performed a detailed investigation of the morphological aspect/ratio of T and L muscles along the arm, particularly in the proximal, medial, and distal arm regions. We wished to determine whether differences in their morphology underlie the preferential use of distinct arm segments during motion (Kennedy et al., 2020). This would ultimately allow us to infer the specialized, and possibly flexible, role played by the octopus arm hydrostatic muscles during motion.

Materials and methods

1. Animal treatment

Twenty *Octopus vulgaris* Cuvier, 1797 specimens were used in this study. Animals of both sexes (weight range: 200–300 g) were collected from local anglers on the Ligurian coast of Italy from October to May. Our research conformed to the ethical principles of the three Rs (replacement, reduction, and refinement) and of minimizing animal suffering, following Directive 2010/63/EU (Italian D. Lgs. n. 26/2014) and the guidelines from Fiorito et al. (Fiorito et al., 2014; Fiorito et al., 2015). All experimental procedures were approved by the institutional board and Italian Ministry of Health (authorization no. 465/2017-PR).

After capture, the animals were placed in 80x50x45 cm aquarium tanks filled with artificial seawater (Tropic Marine) and enriched with sand substrate and clay pot dens. The temperature was maintained constant at 17°C, corresponding to the average temperature at the collection site, and continuously circulated through a biological filter system. Oxygenation was ensured using a dedicated aeration system, and all relevant water chemo/physical parameters were checked daily. Animals were allowed to adapt for at least 5 days before the experiments. They were inspected daily and fed shrimp three times per week. In this study, the octopus arms were labelled in terms of side (left [L] or right [R] from middle to ventral) and position, numbering them in sequence from one to four, following the classical nomenclature (Wells 1978).

Before the experiments, the animals were anesthetized with 3.5% MgCl2 seawater. A short segment was cut from the proximal, medial, and distal portions of one arm per animal (either L2, L3, or R2) and kept in aerated artificial sea water (ASW) (NaCl 460 mM, KCl 10 mM, $MgCl_2$ 55 mM, $CaCl_2$ 11 mM, Hepes 10 mM, glucose 10 mM; pH 7.6) at 4 °C for both histological and biomechanical procedures.

2. Histology

For histological procedures, 15 short arm segments were hand cut with a scalpel from the proximal (~10% of arm length from the base), medial (~50% of arm length from the base), and distal (~95% of arm length from the base) regions of five arms from five different animals.

Arm segments were immediately moved to fresh aerated ASW at 4°C. Samples were fixed overnight in 4% paraformaldehyde (PFA) in ASW, cryopreserved in 30% sucrose overnight, embedded in O.C.T. compound (Electron Microscopy Sciences), and sectioned into 20µm transverse sections with a cryostat microtome (MC5050 Cryostat Microtome).

Transverse sections were treated with standard Nissl staining and mounted on coverslips using DPX mountant (for details see (Maiole et al., 2019)).

Images of the stained sections were acquired in a bright field using an upright microscope (Nikon Eclipse N*i*) and processed using ImageJ software.

The following morphological measurements were collected (when possible standard nomenclature following (Kier and Stella, 2007) was used): the diagonal thickness of the arm (DT), measured as the distance between the axial nerve cord (AN) and the median oblique muscles (OMM); the transverse muscle diagonal extension (TDE), measured as the distance between the AN and the apex of the transverse muscle 'flag' along the DT (see Fig. S1 for details); aboral distance between the AN and external oblique muscle layer (OME) (aboral thickness, AT); oral distance between the AN and OME muscle layer (oral thickness, OT); lateral distance between the AN and OME muscle layer (lateral thickness, LT); thickness of the longitudinal aboral and oral muscles (LA and LO, respectively); transverse aboral and oral muscles (TA and TO, respectively); transverse lateral muscles (TL); longitudinal lateral muscles (LL); internal oblique muscles (OMI); and median oblique muscles (OMM) (see Fig. 1A for a comprehensive description).

3. Muscle biomechanics

General procedure

Forty-two whole arm segments from 15 different animals were hand-cut with a scalpel from one arm proximal-medial portion and immediately moved to fresh aerated ASW. Forty arm muscle strips (length: ~2-5 mm, width: ~1-3 mm, height: ~0.5-1.5 mm) either longitudinal (L) or transverse (T) were then dissected from the aboral side of the whole arm samples. To dissect the L muscles, the epidermis and dermal connective tissue were removed, together with the circumferential and oblique muscle layers. Then, a strip of L muscle was cut out following the proximo-distal axis. To dissect the T muscles, a thin transverse arm slice was cut, and a rectangular strip of the T muscle was isolated following a latero-lateral axis.

At the end of each experimental session, samples were collected and treated for histological procedures as described above. The stained sections were used to estimate the % of orthogonal fibers in each sample.

The muscle strips were immediately mounted in the recording chamber of a dual-mode lever arm system (ASI 300C-LR, Aurora Scientific Instruments) equipped with stimulating bath electrodes. The samples were attached to a micrometer block on one end and to a lever arm on the other using suture threads (silk suture threads 5/0, Ethicon Inc., code: K880H) and tightened with double square knots. The recording chamber was continuously perfused with oxygenated ASW at ~16°C using a peristaltic pump (SJ-1220, Atto Co.). This temperature was in the range of the aquarium tanks in which the animals were maintained and was similar to that of the seawater at the collection site. The muscles were allowed to rest for approximately 10 min in the recording chamber prior to the experiment. Particular care was taken to ensure that the perfusion flux did not induce noise in force recordings. The recordings were digitized and analyzed using a LabVIEW-based data acquisition and analysis system (ASI 604A and 605A, Aurora Scientific Instruments). Data were acquired at a sampling frequency of 10 kHz and filtered using a low-pass filter at 3.3 kHz. At the beginning of the experiment, the resting length (L_R) of the muscle strip was adjusted until a transient passive force was apparent, and it was measured using an electronic caliper as the

distance between the knots. According to current practice (Kier and Curtin, 2002; Milligan et al., 1997), the stimulus strength-twitch response was determined at the beginning of the experiment for each muscle strip (10ms stimuli, 60s interval between successive stimulations). It is worth noting that similar to that observed by Thompson et al. (2014), supramaximal stimulation consistently caused a decrease in the force response; therefore, at the end of the test, we adjusted the stimulus strength to the level employed to reach the maximum force (Thompson et al., 2014). In our experiments, this corresponded mostly to a value of ~900 mA (Fig. 2). Preparations that did not reach maximal stimulation were discarded.

Muscle L_0, defined as the length at which the maximal isometric force (F_0) was recorded, was determined for each sample. During the experimental session, the vitality of the preparation was assessed using isometric contractions at L_0. We set a threshold of 10% maximum force decrease to terminate the experimental session and to exclude data from further analysis.

At the end of the experiment, the height (h) and width (w) of the T and L muscle strips were measured at rest using an electronic caliper under a dissection microscope. The cross-sectional area (CSA) of the samples was calculated assuming that they had a parallelepiped shape (for details see (Di Clemente et al., 2021).

Isometric twitch contraction dynamics

Twelve samples from four different animals were used to characterize T and L twitch contraction dynamics. Muscle strips were stimulated with a single current pulse (10 ms) step stimulation, with the length fixed at L_0. The force-time traces were analyzed offline to obtain the time to peak tension and half relaxation time of each sample. Interestingly, in some samples, we observed after-contraction during the early relaxation phase (Fig. S2 shows an exemplary trace). This interesting phenomenon deserves further investigation. However, in this context, it could influence the calculation of the half-relaxation time and these traces were excluded from the analysis of the relaxation kinetics.

Force-length

Ten samples from four animals were used in this experiment. The force–length relationship was investigated using brief tetanic stimulations (50 Hz, 100ms, 10ms pulse duration) under static strain conditions. Sequential mechanical strain ranging from 1% to 70% of muscle L_R was tested. Muscle strips were lengthened to the desired length using a 2 s long ramp. The preparations were allowed to rest for 20 s and then stimulated (Fig. S3). The resulting force-time traces were analyzed offline using a custom-made MATLAB algorithm to obtain the passive and active components of the force generated by the muscle. Length data were normalized to the optimal muscle length (L_0), and both passive and active components were normalized to sample F_0.

Force-frequency

The force-frequency relationship was investigated under isometric conditions, keeping the muscle length fixed at its L_0. Ten samples from four different animals were tested with 1 s train stimulation (from 1 to 50 Hz , 10 ms pulse duration, 300 s intervals between successive stimulations), as in most cases, shorter durations did not allow samples to reach the maximum plateau force. The peak force generated at each tested frequency was measured offline and used to establish the force-frequency curve. Forces developed at 50 Hz were used to estimate the muscle max tetanic tensions. To allow comparisons between different samples, the data were normalized to the maximal isometric force developed by each muscle strip.

Force-velocity

The force-velocity relationship was investigated using an isotonic protocol on 10 samples from three different animals. The F_0 of each sample was first determined under isometric conditions with brief tetanic stimulations (50 Hz, 100 ms, and 10 ms pulse width) with a fixed length of L_0. The lever arm was then switched to force-clamp mode with imposed loads ranging from 10% to 90% of the sample F_0. A brief tetanic

stimulation (same as above) was delivered at each load with 30 s intervals between different trials. The resulting isotonic shortening (exemplary traces in Fig. S4) was analyzed offline using a custom-made MATLAB algorithm to obtain the shortening velocity, which was normalized for sample L_0.

The force–velocity curves were fitted using Hill's equation in the form expressed in Equation 1:

$$V = V_{max} \cdot F_{max} \frac{F_{max} - F}{G \cdot F + 1} \quad (1)$$

where V is the velocity of shortening (L_0/s), F is the force during shortening normalized to the maximum isometric force, V_{max} is the intercept on the velocity axis, F_{max} is the intercept on the force axis, and G is a constant expressing the curvature. The fitting was performed using the ordinary least squares method and was constrained to have F_{max} = 1.

4. Statistical analysis

Statistical analysis was performed using Prism 8 software (GraphPad Software Inc.) unless otherwise indicated. Data normality was assessed using the Shapiro-Wilk normality test. Comparisons among three or more groups were performed using ordinary one-way ANOVA followed by Tukey's post hoc test.

A Mixed-effects Model was employed to adjust for intra-animal variability when necessary.

Results

1. Muscle aspect/ratio along the arm

Here, the organization of the three main muscle groups of the octopus arm, namely transverse (T), longitudinal (L), and oblique (O) muscles, was analyzed in the proximal, medial, and distal arm segments. Thickness of each muscle group was measured in the oral, aboral, and lateral regions.

No significant differences were observed in the median and internal oblique muscle thicknesses (OMM and OMI, respectively) along the arm (Fig. 1B).

In the arm oral portion, the relative contribution of the T muscles significantly increased in the distal portion (Fig. 1C, one-way ANOVA with Tukey's post hoc test, ***P<0.001), and that of the L muscles showed a comparable decrease toward the distal portion (Fig. 1C, one-way ANOVA with Tukey's post hoc test, *P<0.05).

In the arm aboral portion, the relative thickness of the T muscles was high in the proximal and medial regions and decreased significantly towards the distal end (Fig. 1D, one-way ANOVA, **P<0.01, ***P<0.001), whereas the L muscles were more abundant in the medial and distal regions of the arm and less abundant in the proximal portions (Fig. 1D, one-way ANOVA, *P<0.05).

In the lateral portion of the arm, the thickness of the T muscles was comparable in the proximal and distal portions of the arm, but was significantly lower in the medial arm. Conversely, the L muscles were significantly more abundant in the medial portion, with a decrease in relative thickness more pronounced in the distal part (Fig. 1E, one-way ANOVA, P>0.5).

T muscles occupy the inner portion of the arm, surrounding the axial nerve cord (AN), and are organized in a butterfly-like shape with large muscle bundles entering the longitudinal aboral muscles and the longitudinal lateral muscles and assuming typical 'flag' shapes on the two arm side. The flags on the aboral side connect to the median oblique muscle layer (OMM) through trabeculae of various lengths, depending on the arm segment (proximal, medial, and distal). The extension of the aboral flags was

measured as the transverse diagonal extension (TDE in Fig. 1A and S1) along arm DT and was found to be significantly lower in the distal portion of the arm than in the proximal or medial portions (Fig. 1F, one-way ANOVA with Tukey's post hoc test, *** P<0.001).

2. Biomechanics

The contractile properties of T and L muscles extensively characterized by analyzing: 1) the dynamics of twitch contraction; 2) the force-length relationship; 3) the force-frequency relationship and 4) the force-velocity relationship.

Twitch contraction dynamics

To investigate twitch contraction dynamics of T and L muscles, we analyzed muscle responses to single pulses of stimulation in isometric conditions with muscle strips' length fixed at their L_0. In particular, we compared the time to peak tension and the half-relaxation time of the T and L muscles.

The time to peak tension was significantly different between the two muscles. The average value of L muscle was 59 ± 15 ms and that of T muscle was 107 ± 42 ms (Fig. 3A, mixed-effects model, ***P<0.001). The half relaxation time was also significantly different, with values of 54 ± 12 ms for the L muscles and 165 ± 39 ms for the T muscles (Fig. 3B, mixed-effects model, ***P<0.001). Overall, these results show that T muscles manifest slower twitch contraction dynamics.

Force-length relationship

The capability of the muscle to generate force is highly dependent on its length and is described by the force–length relationship.

Force-length active and passive components from a total of 5 L (black dots) and 5 T (red dots) muscle preparations are shown in figure 4A and B. Passive and active forces were normalized for the samples F_0, plotted against their relative lengths (L/L_0), and fitted with a smoothing spline algorithm (dashed and solid lines in Fig. 4A and B). Both muscles were able to produce significant fractions of their F_0 over a relatively wide range of length (the "plateau" region of the force-length relationship in Fig. 4A and B). No significant differences were observed in the relative active force that the two muscles could exert at their L_R (Fig. 4C, mixed-effects model, $P>0.05$). Additionally, no difference was found in their L_0 (expressed as percentage of the sample L_R) reaching values around the 30% of stretch (32 ± 18 % in T and 26 ± 15 % in L) in both muscle types (Fig. 4D, mixed-effects model, $P>0.05$).

Conversely, the passive forces were remarkably different between the two muscles. In the T muscles, the passive forces manifested a higher relative contribution to the total force generated. At $L_{0,}$ passive forces in L muscle accounted for the 14.65 ± 3.08% of the total sample force while in T muscles this value was 38.64 ± 14.14 % of the total sample force (Fig. 4E, mixed-effects model, ***$P<0.001$).

Force-frequency relationship

The force-frequency relationship is a crucial determinant of muscle function. Slow twitching muscles, which need to sustain prolonged periods of activity, tend to produce higher forces at lower stimulation frequencies. Conversely, fast muscles usually require higher stimulation frequencies to reach plateau forces.

Here, we characterized the force-frequency relationship of the T and L muscles by stimulating isolated muscle strips under isometric conditions at their L_0. Representative traces for L and T are shown in figure 5A; both muscles reached fusion frequencies between 25 and 50 Hz and limited variation of forces occurred at frequencies around 50 Hz. The force–frequency relationship between T and L was found to be significantly different (Fig. 5B, mixed-effects model, **$P<0.01$). Specifically, T muscle force increased more steeply at lower frequencies of stimulation. This might underlie a

possible difference in the physiology of the arm muscles, with T manifesting slower characteristics.

We also measured the twitch-to-tetanus ratio, which, as expected, was significantly higher in T muscles (Fig. 5C, mixed-effects model, ***P<0.001). This last parameter also depends on several properties of the muscle, including the structural properties of the motor unit, such as the number of fibers composing each motor unit, fiber dimensions, and calcium dynamics. While the first parameter is yet to be defined, no evidence has been reported so far on the possible differences in fiber dimension and calcium dynamics in the octopus arm muscles.

The maximal tetanic tension generated by the two muscles at 50 Hz was also different with mean values of 106.9 ± 22.69 $mNmm^{-2}$ for L muscles and 56.77 ± 23.22 $mNmm^{-2}$ for T muscles. It is worth noting that these values are likely to underestimate actual values. As mentioned above, our preparations incorporate fibers oriented orthogonally to the main force vector (that were not less than 17% in L and not less than 21% in T muscles) that did not contribute to the measured tension. Additionally, T muscle fibers are arranged in many directions and, therefore, do not equally contribute to the measured force. Hence, these force values must be taken cautiously, and additional experiments on single fibers are required to obtain a more realistic estimation of the arm muscle fibers forces.

Force-velocity relationship

The force-velocity relationship of T and L muscles was investigated under isotonic conditions imposing loads ranging from 10% to 90% of the maximal isometric force (F_0) of the sample (*see Methods*).

Data were normalized to samples L_0, averaged, plotted, and fitted using Hill's equation to extrapolate V_{max} (Fig. 6). The two curves proved to be significantly different, with L muscles showing higher shortening velocities (Fig. 6, mixed-effects model, ***P<0.001).

The extrapolated V_{max} was also significantly different between the two muscle types (extra sum-of-squares F test, ***P<0.001), with a best-fit value of 0.913 L_0s^{-1} for L

muscles (95% confidence intervals: 0.804-1.043 L_0s^{-1}) and 0.3560 L_0s^{-1} for T muscles (95% confidence interval: 0.2908-0.4414). These velocities reflect not only the intrinsic characteristics of the arm muscle contractile machinery but also the presence of different amounts of fibers oriented in many directions.

Overall, these data show that T muscles have lower contraction and shortening velocities; this, in line with the isometric contraction dynamics and force-frequency relationship results, suggests that they behave as 'slow' muscles compared to L.

Discussion

Motion control of hyper-redundant limbs is currently a hot topic, and several studies have been conducted in the last ten to twenty years, showing the adaptation of octopus arm motor control to various degrees of simplification strategies. These ultimately reduce the demands on the nervous system while still providing remarkable diversity of movement (Gutfreund et al., 1996; Sumbre et al., 2005; Sumbre et al., 2006; Sumbre et al., 2001; Zullo et al., 2011). In this study, we investigated the extent to which dynamic arm deformation can be facilitated by limb-embedded functional properties.

Octopus arms are capable of complex motions that are used in a wide repertoire of behaviors. These complex movements can be produced by a combination of four basic deformations: elongation, shortening, bending (orally, aborally, inward, outward), and torsion (clockwise and counterclockwise) (Kennedy et al., 2020). A fifth important component of arm motion is the arm "stiffening" resulting from the co-contraction of longitudinal (L) and transverse (T) muscles. Stiffening allows the animal to use portions of the arms as dynamic skeletal elements in a variety of behaviors, from walking to reaching and fetching.

Given the cylindrical shape of the arm and its constant volume, longitudinal muscles undergo larger strain variations than transverse muscles. As a result, the lower stiffness of the L muscles may allow the accommodation of the larger range of strains experienced by these muscles during motions. On the other hand, the higher stiffness of

the T muscles may be used to allow resistance to arm diameter increase, a crucial factor required to generate bending over longitudinal compression.

Interestingly, in these motions, arm deformation preferentially occurs within the first 2/3 of the arm corresponding to the proximal-medial arm segments described in this work (Huffard et al., 2005; Levy et al., 2015) Hence, although continuous, the arm manifests a proximo-distal functional specialization. Interestingly, in our study, we found that the two main muscles making up the arm bulk, the L and T muscles, have different morphological aspect ratios along the arm. We showed that L is larger and T is smaller in the aboral medial-distal arm regions. Given the importance of the L muscles in bending, this might correspond to the highest rate of bend formation occurring in these arm segments (Kennedy et al., 2020). We also found that the aboral transverse diagonal extension of the transverse muscle, is maximal at proximal-medial regions. This might be in line with the observation that arm elongation, which is driven by the decrease in diameter induced by T muscle contraction, occurs preferentially in the proximal region of the arm (Kennedy et al., 2020 Huffard et al., 2005; Levy et al., 2015). Thus, activation of muscles from different regions of the arm may produce various types of movements. Conversely, oblique muscles that support motions such as arm twisting, occurring along the entire arm length (Kennedy et al., 2020), manifest a uniform distribution throughout the arm.

Several examples of functional specialization can be found in both vertebrates and invertebrates, where even different anatomical regions in single muscles may serve a variety of functions (Ahn et al., 2018; Ting and Chiel, 2017). For instance, in the cat hind limb muscles, the biceps femoris is involved in slow walking, whereas the posterior regions are recruited during faster motions (Chanaud and Macpherson, 1991). Likewise, in the buccal retractor muscle of the invertebrate *Aplysia californica*, the anterior and posterior parts are activated and used differently during feeding behavior (McManus et al., 2014). These anatomical organizations can also be paralleled by differences in the muscle biomechanics.

This seems to be the case for the octopus arm, as we showed that the T and L muscles intrinsically differ in their active biomechanical properties.

Specifically, we found that T muscles manifest slow activation properties and relaxation kinetics typical of skeletal slow-twitch muscles, such as the soleus (Hessel and Joumaa, 2019). They may thus be adapted to sustain strong and prolonged period of activity and to work as “postural” muscles. Conversely, the L muscles show faster characteristics typical of skeletal fast-twitch muscles, such as the extensor digitorum longus (Hessel and Joumaa, 2019), which supports their involvement in finely tuned movements, such as bending and manipulation, typical of the octopus arms.

Interestingly, both T and L muscles show similarities in activation properties and relaxtion/contraction kinetics to the transverse musculature of the squid arm, but not to the tentacle (see Table S1). However, we should consider that no information is currently available on the biomechanics of the squid longitudinal muscles. Similar to other cephalopod hydrostatic organs, the T and L muscles were able to produce significant fractions of their maximal force over a wide range of lengths (Milligan et al., 1997; Thompson et al. 2014), and they did not substantially differ in the active force-length relationships. We also showed that the maximal tetanic force of the T muscles was lower than that recorded in other cephalopod muscle limbs. This might be due to the presence in this type of muscle, of a large amount of fibers oriented in many directions (including orthogonal fibers not contributing to the force estimated). Moreover, we cannot exclude the possibility that a variation in the protein of the contractile machinery might also exist and account, at least partially, for the differences observed. In order to elucidate this point, single muscle fiber force measurements and proteomic analysis of arm muscles can be further envisaged.

Altogether, we suggest that the octopus arm muscles behave as slow or fast muscles based on their passive and active properties.

In line with what shown in Di Clemente et al. (Di Clemente et al., 2021), T and L also showed significant differences in their passive force component, which was significantly larger in T muscles. Passive forces in the arm muscles are due to the massive presence of coiled elastic fibers (see Fig. S5), arranged differently in the two muscles and

supporting the arm passive response to deformations (Di Clemente et al., 2021). Compared to typical vertebrate muscles, the L and T muscles manifest passive properties similar to skeletal and cardiac muscles, respectively (Feher, 2012). Passive mechanical properties are major determinants of cardiac function and are due to the composition of titin, collagen, and intermediate filaments (Emig et al., 2021; Granzier and Irving, 1995). In skeletal muscles, passive components contribute less to the total tension and are mainly due to the tendons and extracellular matrix. These not only work as elastic elements, but together with bones, hold muscles to a resting length that is close to their optimal, at which the production of tension is maximized (Konow et al., 2012; Roberts, 2016).

Intuitively, this situation is significantly different for hydrostatic bodies. The complete absence of any internal or external rigid skeletal elements endows muscles with unprecedented freedom. In contrast, the presence of internal hydrostatic pressure may influence muscle contractile forces and response to deformation (Kier, 2020; Sleboda and Roberts, 2019).

Di Clemente et al. showed that intrinsic tensional stress within the arm causes T and L muscles to be held under different strain conditions in the arm at rest. Hence, they will operate on different regions of their force-length relationship, with T muscles closer to their L_0 and L muscles farther away from it, and they will produce different amounts of force when activated (Fig.7). Thus, the same type of motor neuronal input reaching T or L can induce different responses depending on the strain level. This allows the same muscle to become functionally different, thereby providing an intelligent mechanism to increase its flexibility in use.

What is the functional significance of this difference in operating length? Why should it be convenient to hold a muscle in a non-optimal length range? Perhaps we should consider the following: Muscles have not been evolved only to generate power but also to ‘stabilize’ posture, regulate the fine execution of movement and, in the case of hydrostatic limbs, to support the structure through stiffening. This is achieved through both contractile and elastic elements of the muscle, the latter being very relevant in hydrostatic limbs, acting synergistically in the body musculature.

To illustrate this concept, we will dissect one exemplary octopus arm motion point-by-point: the arm extension. Arm extension starts with the formation of a bending point along the first 2/3 of the arm, preferentially in the lateral and aboral-up directions (Kennedy et al., 2020). The significant reduction in T elements at the oral side of the arm preferentially favors bend formation in this direction, thus allowing the suckers to be directly exposed to the probing environment. Bend production is due to the contraction of the T and L muscles on one side of the arm, with concomitant elongation of the L muscles on the opposite side. This would induce elastic forces of both T (on the bending site) and L (on the side opposite to bending) to be 'released', hence reducing the energetic cost for bending.

Upon bend formation, arm extension is generated through gradual stiffening of the arm, which propels the bend towards the arm tip (Gutfreund et al., 1998; Gutfreund et al., 1996; Sumbre et al., 2001).

Arm stiffening is achieved through the co-contraction of the T and L muscles. During this process we can expect, based on the configuration of the passive elastic elements, T muscles to be 'favored' in contraction while L muscles to be disfavored thus possibly producing a canceling effect of their elastic forces. Finally, and perhaps not least important, arm reconfiguration after extension (arm returning to its resting state) might be reached, at reduced cost, simply by stopping muscle contraction, thus allowing for passive redistribution of strain along the arm. Notably, the possibility of generating stiffening in selective muscle layers of hydrostatic muscles, have also profound implications in motor control strategies as stiffened muscles can be used as artificial 'skeletons' against which other muscles can act through contraction (Hooper, 2006; Kier, 2012).

Additionally, in soft tissue structures, the expansion or contraction of one muscle can significantly affect the surrounding muscles. For instance, changing the shape of one muscle can alter the mechanical advantage of other muscles, enhancing or reducing their ability to produce force (Novakovic et al. 2006). Therefore, the contribution of arm muscles to specific behaviors is the result of a fine interplay between their physiological

properties, morphological arrangement, and anatomical positioning, allowing muscles to move relative to one another and produce different motions.

The existence of arm regionalization, together with the muscle-specific biomechanical properties, represents an arm-embedded readily accessible system for a neural motor code to reconfigure the limb without the need for a complex feed-forward process. Thus, it may be an additional simplification strategy developed to further reduce the complexity of controlling highly flexible structures.

Conclusion

Here, we show that although continuous, octopus arms are endowed with a certain degree of regional specialization, where the arm muscles manifest different biomechanical properties. However, adaptation of arm muscle physiology is only part of a scenario in which muscle embedding and regionalization play an important role in the determination of muscle use during specific tasks. The type of motion produced by the arm is linked to the type of muscle activated, its initial state, and the specific arm region involved.

Thus, to have a comprehensive understanding of octopus arm motor performances, muscle activation and biomechanical properties need to be interpreted in light of their embedding and anatomical organization within the arm. This consideration is particularly relevant in the field of bio-robotics, as it may provide important insights into both the construction and activation of artificial soft elements while leveraging their control architecture (Kang et al., 2016; Zullo et al., 2012).

Taken together, our results support the idea that cephalopods are distinguishable animals that have used simplification strategies, based on multifunctional design constraints, to control hyper-redundant limbs and bodies in a large variety of environmental niches (Hanlon and Messenger, 2018; Ponte et al., 2021). Thus, we can consider the octopus as an ensemble of well-coordinated effectors, from neural organization to body constraints.

Acknowledgements

We thank Benny Hochner for valuable discussions, Giacomo Pruzzo for technical assistance, Dr. Marcello Ceppi for valuable statistical assistance and the animal care and maintenance facility of the IRCCS, San Martino Hospital of Genoa.

Competing interests

The authors declare no competing interests.

Funding

This work was supported by the Seventh Framework Programme (OCTOPUS IP, Project Number FP7-231608), European Cooperation in Science and Technology (FA 1301 CephsInAction), and Office of Naval Research (award number N00014-21-1-2516).

Data availability

Data will be made available upon request.

List of symbols and abbreviations

AN = axial nerve cord

ASW = artificial sea water

AT = aboral thickness

CSA = cross-sectional area

DT = diagonal thickness

F/L = force-length

F/V = force-velocity

F_{max} = maximal force

L = longitudinal

L_0 = resting length of the muscle once dissected from the arm

LA = longitudinal aboral muscles

LL = longitudinal lateral muscles

LT = lateral thickness

O = oblique

OME= external oblique muscles

OMI= internal oblique muscles

OMM= median oblique muscles

OT = oral thickness

PFA = Paraformaldehyde

RM = repeated measures

T = transverse

TA = transverse aboral muscles

TDEI = transverse diagonal extension

TL = transverse lateral muscles

Author contributions

A.D.C., L.Z. and F. M. performed the experiments; L.Z. and A.D.C. wrote the manuscript; L.Z. designed the project and supervised the work.

References

Burkholder, T. J. and Lieber, R. L. (2001). Sarcomere length operating range of vertebrate muscles during movement. *J Exp Biol* **204**, 1529-36.

Di Clemente, A., Maiole, F., Bornia, I. and Zullo, L. (2021). Beyond muscles: role of intramuscular connective tissue elasticity and passive stiffness in octopus arm muscle function. **224**.

Emig, R., Zgierski-Johnston, C. M., Timmermann, V., Taberner, A. J., Nash, M. P., Kohl, P. and Peyronnet, R. (2021). Passive myocardial mechanical properties: meaning, measurement, models. **13**, 587-610.

Feher, J. (2012). 5.7 - The Cellular Basis of Cardiac Contractility. In *Quantitative Human Physiology*, (ed. J. Feher), pp. 477-485. Boston: Academic Press.

Fiorito, G., Affuso, A., Anderson, D. B., Basil, J., Bonnaud, L., Botta, G., Cole, A., D'Angelo, L., De Girolamo, P., Dennison, N. et al. (2014). Cephalopods in neuroscience: regulations, research and the 3Rs. *Invert Neurosci* **14**, 13-36.

Fiorito, G., Affuso, A., Basil, J., Cole, A., de Girolamo, P., D'angelo, L., Dickel, L., Gestal, C., Grasso, F., Kuba, M. et al. (2015). Guidelines for the Care and Welfare of Cephalopods in Research –A consensus based on an initiative by CephRes, FELASA and the Boyd Group. *Laboratory Animals* **49**, 1-90.

Fossati, S. M., Benfenati, F. and Zullo, L. (2011). Morphological characterization of the Octopus vulgaris arm. Vie Milieu 61, 197-201.

Granzier, H. L. and Irving, T. C. (1995). Passive tension in cardiac muscle: contribution of collagen, titin, microtubules, and intermediate filaments. *Biophys J* **68**, 1027-44.

Gutfreund, Y., Flash, T., Fiorito, G. and Hochner, B. (1998). Patterns of arm muscle activation involved in octopus reaching movements. *J Neurosci* **18**, 5976-87.

Gutfreund, Y., Flash, T., Yarom, Y., Fiorito, G., Segev, I. and Hochner, B. (1996). Organization of octopus arm movements: a model system for studying the control of flexible arms. *J Neurosci* **16**, 7297-307.

Gutnick, T., Byrne, Ruth A., Hochner, B. and Kuba, M. (2011). Octopus vulgaris Uses Visual Information to Determine the Location of Its Arm. *Current Biology* **21**, 460-462.

Gutnick, T., Zullo, L., Hochner, B. and Kuba, M. J. (2020). Use of Peripheral Sensory Information for Central Nervous Control of Arm Movement by Octopus vulgaris. *Current Biology*.

Hanlon, R. and Messenger, J. (2018). Cephalopod Behaviour.

Hessel, A. L. and Joumaa, V. (2019). Optimal length, calcium sensitivity and twitch characteristics of skeletal muscles from mdm mice with a deletion in N2A titin. **222**.

Hooper, S. L. (2006). Motor control: the importance of stiffness. *Curr Biol* **16**, R283-5.

Huffard, C. L., Boneka, F. and Full, R. J. (2005). Underwater bipedal locomotion by octopuses in disguise. *Science* **307**, 1927.

Kang, R., Guglielmino, E., Zullo, L., Branson, D. T., Godage, I. and Caldwell, D. G. (2016). Embodiment design of soft continuum robots. *Advances in Mechanical Engineering* **8**, 1687814016643302.

Kennedy, E. B. L., Buresch, K. C., Boinapally, P. and Hanlon, R. T. (2020). Octopus arms exhibit exceptional flexibility. *Scientific Reports* **10**, 20872.

Kier, W. M. (2012). The diversity of hydrostatic skeletons. *J Exp Biol* **215**, 1247-57.

Kier, W. M. (2016). The Musculature of Coleoid Cephalopod Arms and Tentacles. *Front Cell Dev Biol* **4**, 10.

Kier, W. M. (2020). Muscle force is modulated by internal pressure. *Proc Natl Acad Sci U S A*.

Kier, W. M. and Curtin, N. A. (2002). Fast muscle in squid (Loligo pealei): contractile properties of a specialized muscle fibre type. *The Journal of Experimental Biology* **205 Pt 13**, 1907-16.

Kier, W. M. and Stella, M. P. (2007). The arrangement and function of octopus arm musculature and connective tissue. *J Morphol* **268**, 831-43.

Konow, N., Azizi, E. and Roberts, T. J. (2012). Muscle power attenuation by tendon during energy dissipation. *Proc Biol Sci* **279**, 1108-1113.

Levy, G., Flash, T. and Hochner, B. (2015). Arm coordination in octopus crawling involves unique motor control strategies. *Curr Biol* **25**, 1195-200.

Maiole, F., Tedeschi, G., Candiani, S., Maragliano, L., Benfenati, F. and Zullo, L. (2019). Synapsins are expressed at neuronal and non-neuronal locations in Octopus vulgaris. *Scientific Reports* **9**, 15430.

Milligan, B., Curtin, N. and Bone, Q. (1997). Contractile properties of obliquely striated muscle from the mantle of squid (Alloteuthis subulata) and cuttlefish (Sepia officinalis). *Journal of Experimental Biology* **200**, 2425-2436.

Ponte, G., Taite, M., Borrelli, L., Tarallo, A., Allcock, A. L. and Fiorito, G. (2021). Cerebrotypes in Cephalopods: Brain Diversity and Its Correlation With Species Habits, Life History, and Physiological Adaptations. *Frontiers in Neuroanatomy* **14**.

Richter, J. N., Hochner, B. and Kuba, M. J. (2015). Octopus arm movements under constrained conditions: adaptation, modification and plasticity of motor primitives. *The Journal of Experimental Biology* **218**, 1069.

Roberts, T. J. (2016). Contribution of elastic tissues to the mechanics and energetics of muscle function during movement. *J Exp Biol* **219**, 266-75.

Sleboda, D. A. and Roberts, T. J. (2019). Internal fluid pressure influences muscle contractile force. *Proc Natl Acad Sci U S A*.

Sumbre, G., Fiorito, G., Flash, T. and Hochner, B. (2005). Neurobiology: motor control of flexible octopus arms. *Nature* **433**, 595-6.

Sumbre, G., Fiorito, G., Flash, T. and Hochner, B. (2006). Octopuses use a human-like strategy to control precise point-to-point arm movements. *Curr Biol* **16**, 767-72.

Sumbre, G., Gutfreund, Y., Fiorito, G., Flash, T. and Hochner, B. (2001). Control of octopus arm extension by a peripheral motor program. *Science* **293**, 1845-8.

Taylor, J. and Kier, W. (2003). Switching Skeletons: Hydrostatic Support in Molting Crabs. *Science (New York, N.Y.)* **301**, 209-10.

Thompson, J. T., Shelton, R. M. and Kier, W. M. (2014). The length-force behavior and operating length range of squid muscle vary as a function of position in the mantle wall. *J Exp Biol* **217**, 2181-92.

Uyeno, T. A. and Kier, W. M. (2005). Functional morphology of the cephalopod buccal mass: a novel joint type. *J Morphol* **264**, 211-22.

Zullo, L., Chiappalone, M., Martinoia, S. and Benfenati, F. (2012). A "spike-based" grammar underlies directional modification in network connectivity: effect on bursting activity and implications for bio-hybrids systems. *PLoS One* **7**, e49299.

Zullo, L., Fossati, S. M. and Benfenati, F. (2011). Transmission of sensory responses in the peripheral nervous system of the arm of Octopus vulgaris. *Vie et Milieu* **61**, 197-201.

Zullo, L., Fossati, S. M., Imperadore, P. and Nodl, M. T. (2017). Molecular Determinants of Cephalopod Muscles and Their Implication in Muscle Regeneration. *Front Cell Dev Biol* **5**, 53.

Zullo, L. and Hochner, B. (2011). A new perspective on the organization of an invertebrate brain. *Commun Integr Biol* **4**, 26-9.

Zullo, L., Sumbre, G., Agnisola, C., Flash, T. and Hochner, B. (2009). Nonsomatotopic Organization of the Higher Motor Centers in Octopus. *Current Biology* **19**, 1632-1636.

Figures

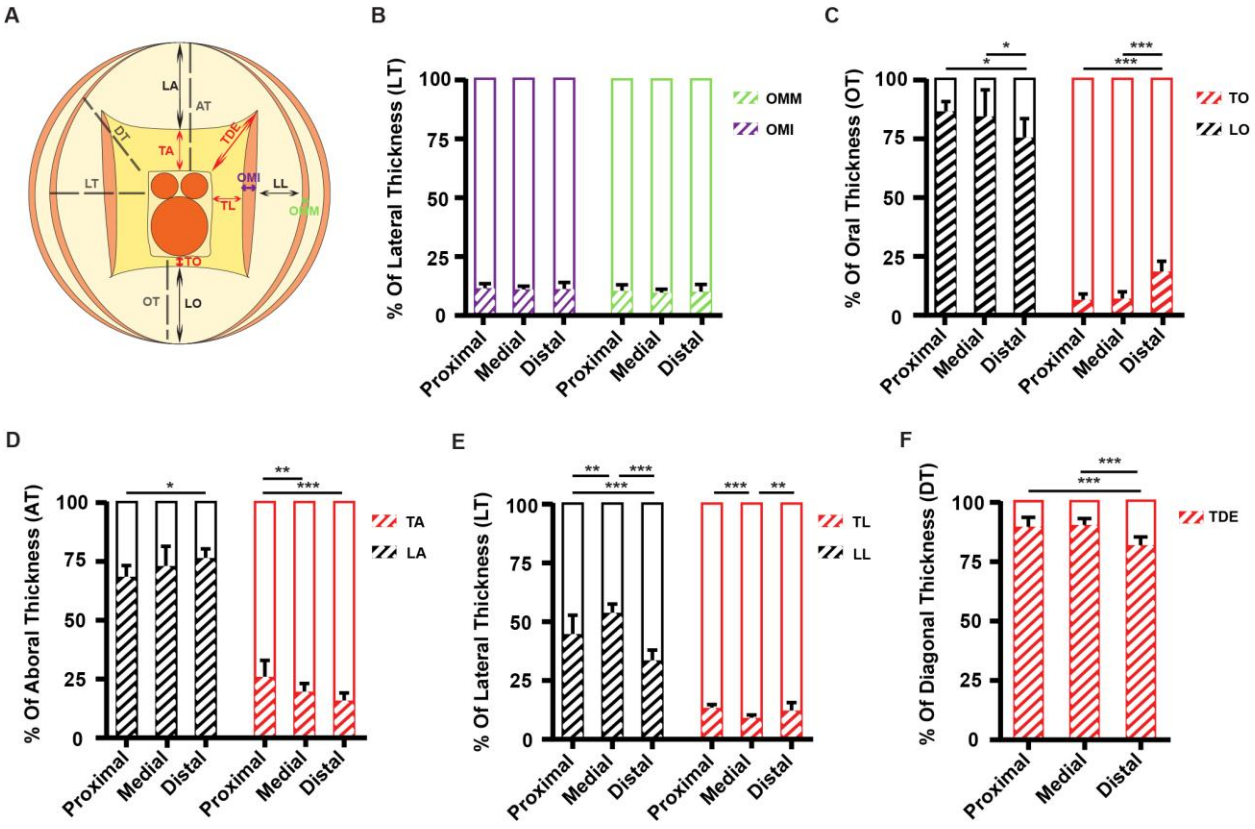

Figure 1. Muscle aspect ratio along the arm. **(A)** Schematic representation of an arm transverse section with reference to the measurements obtained: DT = diagonal thickness, TDE = transverse diagonal extension, OT = oral thickness, LO = longitudinal oral, TO = transverse oral, AT = aboral thickness, LA = longitudinal aboral, TA = transverse aboral, LT = lateral thickness, LL = longitudinal lateral, TL = transverse lateral, OMM = median oblique muscles, OMI = inner oblique muscles. Bars show mean ± SD **(B)** Relative lateral thickness of OMI ($n_{proximal}$ = 10, n_{medial} = 10, n_{distal} = 10; one-way ANOVA with Sidak's post hoc test, P>0.05) and OMM muscles ($n_{proximal}$ = 12, n_{medial} = 12, n_{distal} = 12; one-way ANOVA with Sidak's post hoc test, P>0.05). **(C)** Relative oral thickness of L ($n_{proximal}$ = 8, n_{medial} = 12, n_{distal} = 10; one-way ANOVA with Sidak's post hoc test, *P<0.05) and T muscles ($n_{proximal}$ = 11, n_{medial} = 14, n_{distal} = 13; one-way ANOVA with Sidak's post hoc test, ***P<0.001). **(D)** Relative aboral thickness of L

($n_{proximal}$ = 9, n_{medial} = 14, n_{distal} = 14; one-way ANOVA with Sidak's post hoc test, *P<0.05) and T muscles ($n_{proximal}$ = 10, n_{medial} = 14, n_{distal} = 14; one-way ANOVA with Sidak's post hoc test, ***P<0.001, **P<0.01). **(E)** Relative lateral thickness of the L ($n_{proximal}$ = 10, n_{medial} = 11, n_{distal} = 11; one-way ANOVA with Sidak's post hoc test, ***P<0.001, **P<0.01) and T muscles ($n_{proximal}$ = 13, n_{medial} = 12, n_{distal} = 13; one-way ANOVA with Sidak's post hoc test, ***P<0.001, **P<0.01). **(F)** TDE relative length ($n_{proximal}$ = 8, n_{medial} = 7, n_{distal} = 10; one-way ANOVA with Sidak's post hoc test, ***P<0.001).

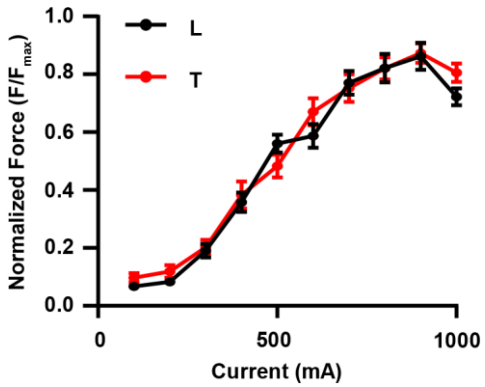

Figure 2. Stimulus strength-twitch response of the L and T muscles. Data are presented as mean ± SEM (n = 15 for both experimental groups).

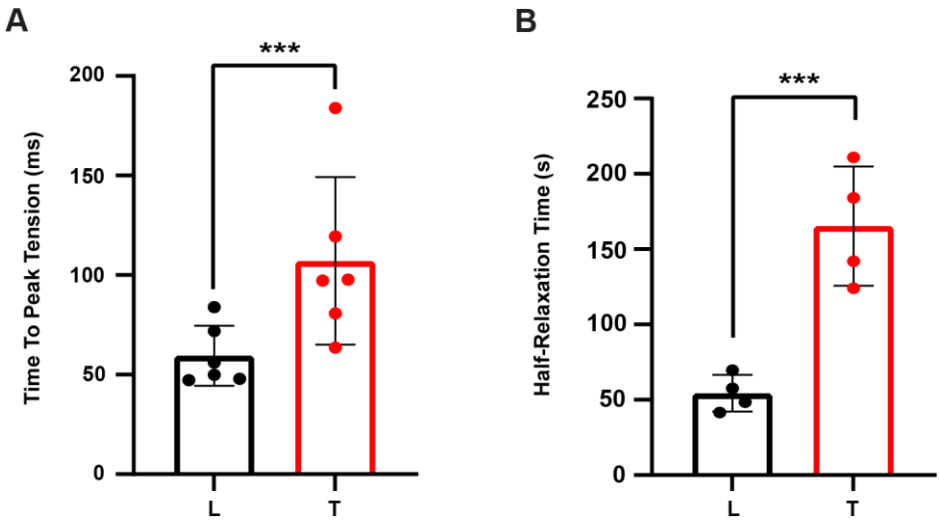

Figure 3. Twitch contraction dynamics. (A) Time to peak tension (mixed-effects model, ***P<0.001, n = 6 for both experimental groups). **(B)** Half-relaxation time (mixed-effects model, ***P<0.001, n = 4 for both experimental groups).

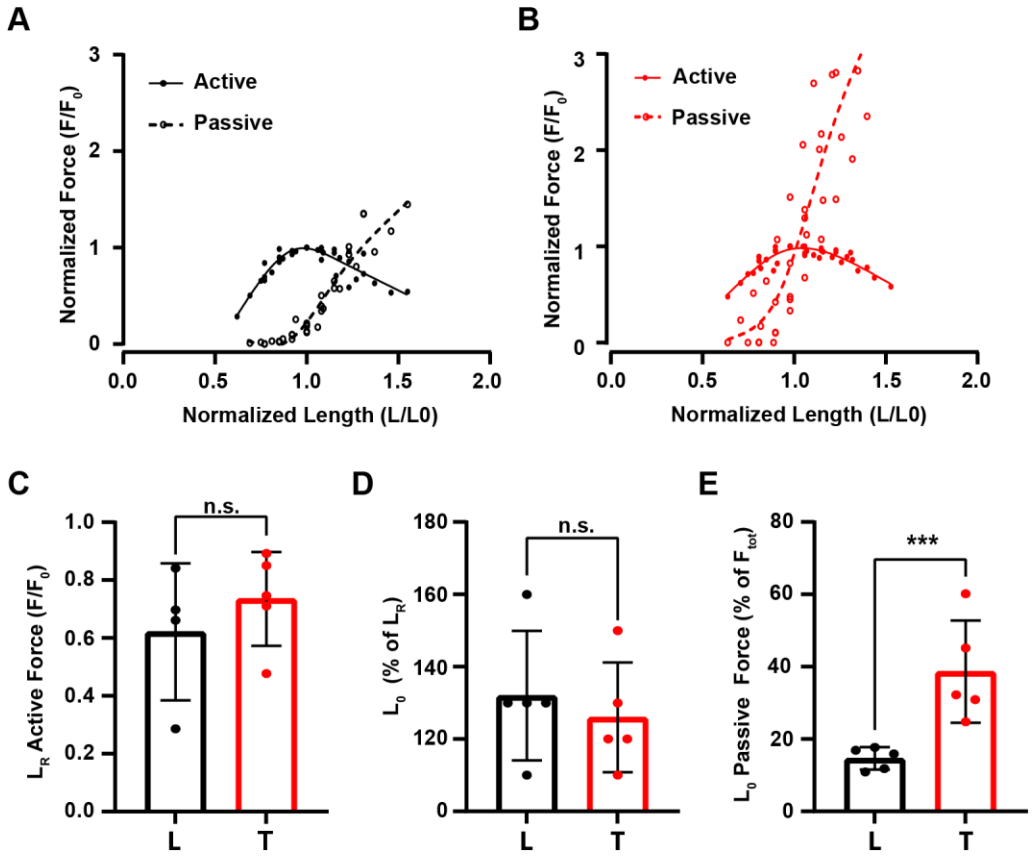

Figure 4. Force-length relationship. (A) Passive and active force-length relationship of the L muscles. All data points from n = 5 samples are represented. Data were normalized for the sample F_0 and L_0 and fitted with a smoothing spline algorithm (dashed and solid lines in figure). Data fitting was only descriptive. **(B)** Passive and active force-length relationship of the T muscles. All data points from n = 5 samples are presented. The data were normalized for sample F_0 and L_0 and fitted with a smoothing spline algorithm (dashed and solid lines in the figure). Data fitting was only descriptive. **(C)** Relative force of the L and T muscles at their L_R (F_R) expressed as a fraction of sample F_0. No significant differences were found between the two muscles (mixed-effects model, P>0.05, n_{long} = 4, n_{trans} = 5. **(D)** L and T muscle strips' L_0 expressed as percentage of their L_R. No significant differences were found between the two muscles (mixed-effects model, P>0.05, n = 5 for both experimental groups). Bars show mean ± SD. **(E)** Passive contribution to the total force developed by the L and T muscle strips at L_0. The T muscles showed a significantly higher contribution of passive forces compared to the L (mixed-effects model, ***P<0.001, n = 5 for both experimental groups). Bars show mean ± SD.

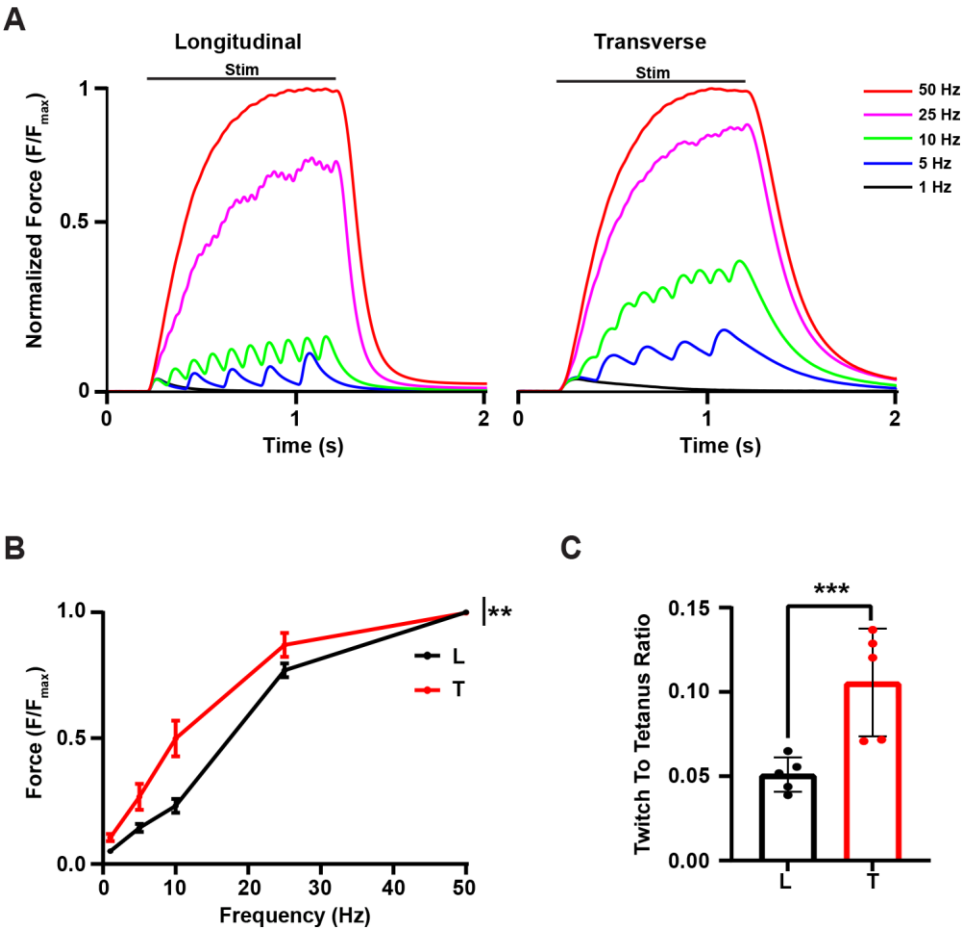

Figure 5. Force-frequency relationship. (A) Representative force-time traces from one L (left) and one T (right) sample normalized to their maximal isometric force. Stimulus duration is indicated. **(B)** Average force-frequency curve of T and L muscles. Data are represented as mean ± SEM. The T muscles were able to exert higher fractions of their maximal forces at lower frequency of stimulation (mixed-effects model, **P<0.01, n = 5 for both experimental groups). **(C)** Twitch-to-tetanus ratio was significantly higher in T muscles (mixed-effects model, ***P<0.001, n = 5 for both experimental groups). The rectangular bar shows the mean values.

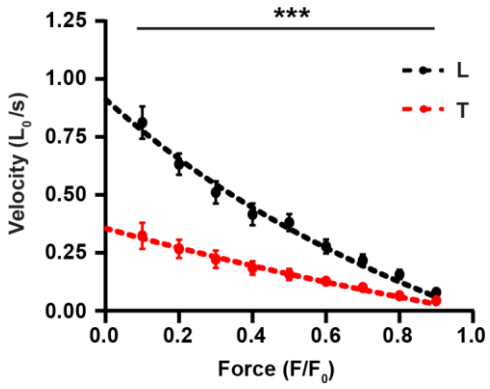

Figure 6. Force-velocity relationship. The force and velocity were normalized for F_0 and L_0 respectively. Data are represented as mean ± SEM. The dashed lines represent the Hill's fitting of the curves. L muscles showed significantly higher shortening velocities than T muscles (mixed-effects model, ***P<0.001, n = 5 for both experimental groups).

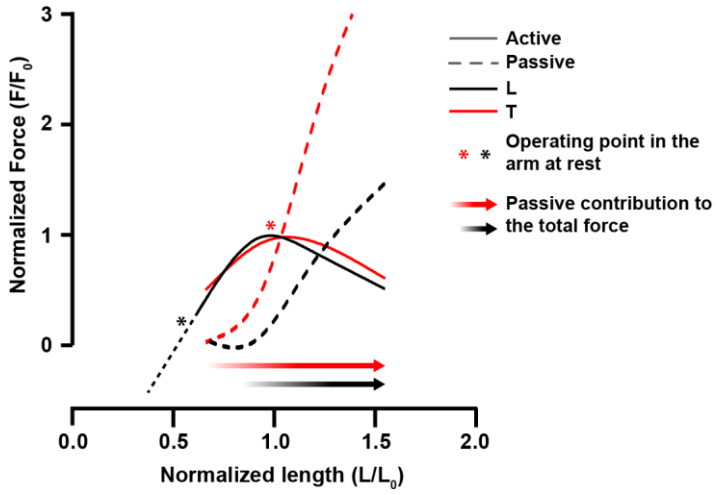

Figure 7. Shift in muscles operating length in an intact arm. Spline fitting of passive and active force-length relationships have been reported for T and L muscles. Black and red asterisks indicate the operating points of T and L in an arm at rest based on the tensional stress reported by Di Clemente et al. (Di Clemente et al., 2021). It is worth noting that the passive tension of the T muscle (red arrow) is greater at shorter lengths, while the L passive tension begins to rise at values close to its L_0 (black arrow). Altogether, this suggest that although T and L do not manifest major differences in their active force-length curves, their strain level allows them to work in different regions of their force-length curve and produce variable amounts of forces.

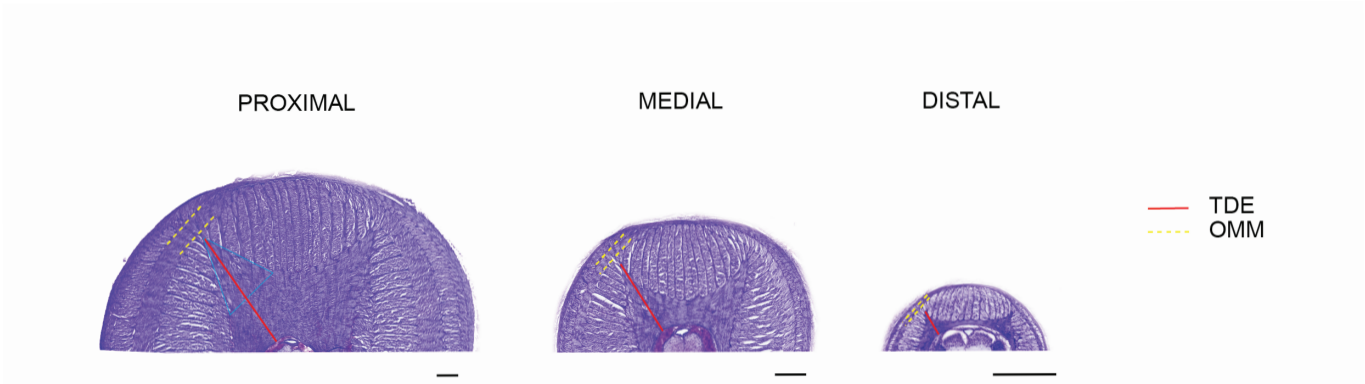

Fig. S1. Representative photomicrographs of details of the arm proximal, medial and distal sections. Blue lines show the location of a transverse muscle 'flag' composed by a large bundle of fibers entering the longitudinal aboral (and oral) muscles and longitudinal lateral muscles. The flags on the aboral side connect to the median oblique muscle layer (OMM; yellow dashed lines) through trabeculae of various lengths depending on the arm segment (proximal, medial, distal). The diagonal extension of the transverse muscle (TDE) in the three arm segments is shown in red. Scale bar 500 µm.

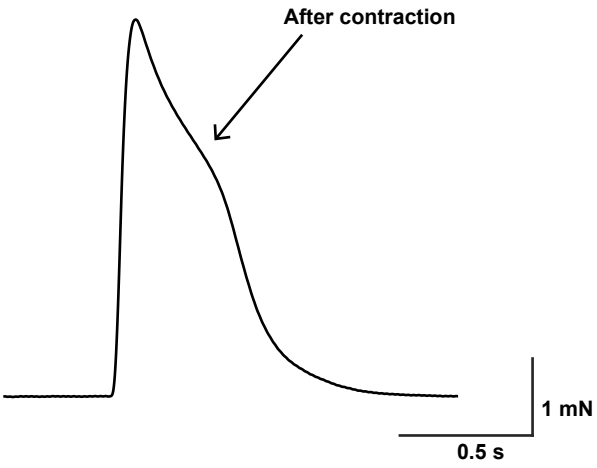

Fig. S2. After contraction. Representative isometric twitch force-time trace were the after contraction phenomenon is evident.

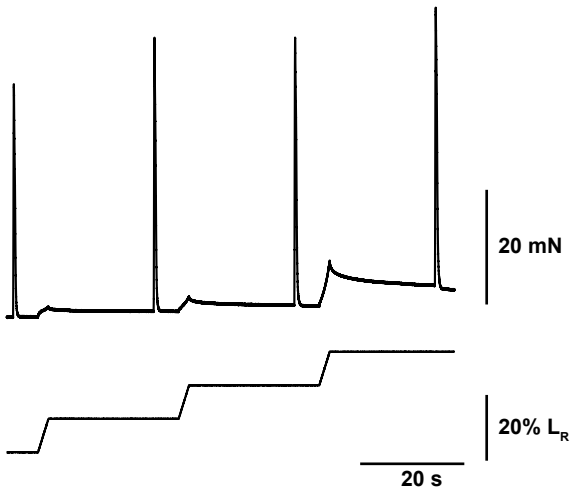

Fig. S3. Force-length protocol and representative trace. Upper panel: force-time traces corresponding to the position-time traces in the lower panel. Lower panel: position-time traces with length-ramp protocols at increasing amplitudes (expressed as a percentage of L0).

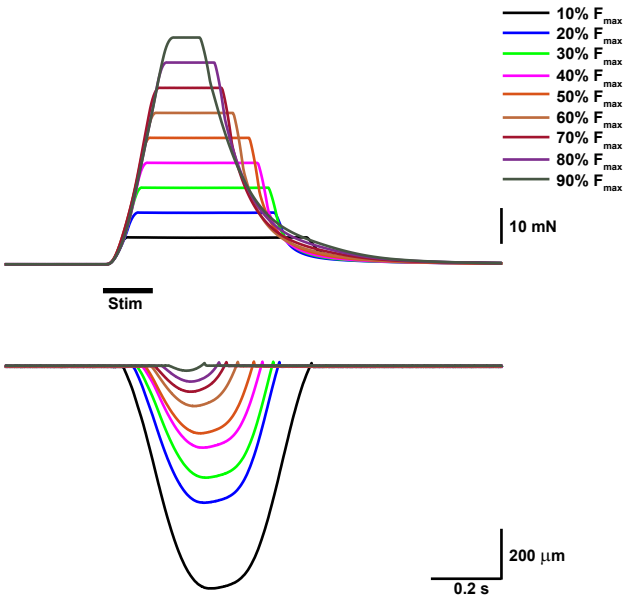

Fig. S4. Force-velocity protocol and representative traces. Upper panel: force-time representative traces. Train stimulation is indicated by a black bar below the traces. Lower panel: position-time traces.

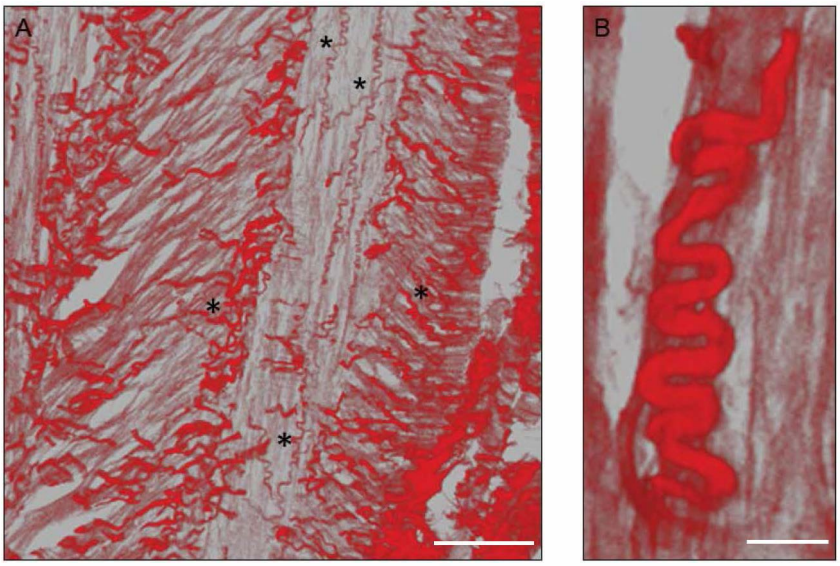

Fig. S5. (A) Details of an arm transverse slice stained with picrosirius red where many coiled elastic fibers (asterisks) are visible. Scale bar = 100 μm (B) Magnified view of one elastic fiber. Scale bar = 25 μm

Table S1. Comparison between contractile properties of squid and octopus arms. HRT = half-relaxation time, TTP = time to peak tension. Data are presented as mean ± SD. CI: 95% confidence interval.

Parameters	**SQUID (*Loligo pealei*)**			**OCTOPUS (*Octopus vulgaris*)**	
	T arm	T tentacle	References	T	L
Shortening velocity	1.47±0.22	15.38±0.97	Kier and Curtin, 2002	0.356 (CI: 0.804 to 1.043)	0.913 (CI: 0.291 to 0.441)
Twitch:tetanus	0.03±0.02	0.66±0.06	Kier and Curtin, 2002	0.1056±0.0319	0.051±0.010
HRT	153.4±65.9	52.7±7.3	Kier and Curtin 2002	165.3±39.51	54.30±12.18
TTP	59.6±10.2	33.6±3.0	Kier and Curtin, 2002	107.2±42.04	59.53±15.09